# Multinucleon transfer in the $^{136}$Xe + $^{208}$Pb reaction

Cheng Li,[1,2,*] Fan Zhang,[1,2] Jingjing Li,[1,2] Long Zhu,[3] Junlong Tian,[4,†] Ning Wang,[5,‡] and Feng-Shou Zhang[1,2,6,§]

[1]*The Key Laboratory of Beam Technology and Material Modification of Ministry of Education, College of Nuclear Science and Technology, Beijing Normal University, 100875 Beijing, China*

[2]*Beijing Radiation Center, Beijing 100875, China*

[3]*Sino-French Institute of Nuclear Engineering and Technology, Sun Yat-sen University, Zhuhai 519082, China*

[4]*School of Physics and Electrical Engineering, Anyang Normal University, Anyang 455000, China*

[5]*Department of Physics, Guangxi Normal University, Guilin 541004, China*

[6]*Center of Theoretical Nuclear Physics, National Laboratory of Heavy Ion Accelerator of Lanzhou, Lanzhou 730000, China*

(Received 3 November 2015; revised manuscript received 22 December 2015; published 25 January 2016)

The dynamic mechanics in the multinucleon transfer reaction $^{136}$Xe + $^{208}$Pb at an incident energy of $E_{\mathrm{c.m.}} =$ 450 MeV is investigated by using the improved quantum molecular dynamics model (ImQMD). The lifetime of the neck directly influences the nucleon exchange and energy dissipation between the projectile and the target. The total-kinetic-energy–mass distributions and excitation energy division of primary binary fragments and the mass distributions of primary fragments at different impact parameters are calculated. The thermal equilibrium between two reaction partners has been observed at the lifetime of a neck larger than 480 fm/$c$. By using the statistical decay code GEMINI to describe the de-excitation process of the primary fragments, the isotope production cross sections from Pt to At are compared with the prediction by the dinuclear system and GRAZING model. The calculations indicate that the GRAZING model is suitable for estimating the isotope production cross sections only for $\Delta Z = -1$ to $+2$; the DNS + GEMINI calculations underestimate the cross sections in the neutron-rich and neutron-deficient regions; and the ImQMD + GEMINI calculations give reasonable predictions of the isotope production cross sections for $\Delta Z = -3$ to 0.

DOI: 10.1103/PhysRevC.93.014618

## I. INTRODUCTION

The multinucleon transfer reaction is a typical mechanism in heavy-ion collisions at incident energies close to the Coulomb barrier. Many such experiments were performed in the late 1970s and 1980s [1–7]. They provided valuable information on the nucleon-nucleon correlation in nuclei, neutron flow in the neck, transition from the quasielastic to the deep-inelastic regime, and interplay of nuclear reactions and structure, etc. Multinucleon transfer reactions are also extremely important for producing superheavy nuclei and neutron-rich heavy nuclei. For example, the production of neutron-rich trans-target nuclides up to Fm and Md with cross sections at the 0.1 $\mu$b level were synthesized in near-barrier collisions of $^{238}$U + $^{248}$Cm [4]. The neutron-rich heavy isotopes $^{203}$Au and $^{205}$Au were discovered with cross sections 362 and 52 $\mu$b, respectively, in 1994 by Wennemann *et al.* through a deep-inelastic reaction from an 11.4 MeV/u $^{208}$Pb beam accelerated by the UNILAC accelerator bombarding on a natural tungsten target [8]. So far, among the elements with $Z > 100$ only neutron-deficient isotopes (located at the left side of the stability line) have been produced by using cold fusion [9] and hot fusion [10,11] reactions due to the limitation of the neutron number of available projectiles and targets. For the heavy elements located in the "north-east" part of the nuclear map, only a few neutron-rich isotopes have been found and most of them are produced by means of cold fragmentation of projectile. For example, the neutron-rich isotopes $^{202,203,204}$Pt can be produced by using a 1 GeV/$A$ $^{208}$Pb beam impinged on a $^{9}$Be target at GSI [12]. However, the production cross sections in this reaction are less than the expected value in the low-energy multinucleon transfer reactions. Due to the limitations of fragmentation and fusion reactions the multinucleon transfer reaction has attracted renewed attention in recent years for the production of new neutron-rich heavy and superheavy nuclei [13–20]. For a comprehensive review of multinucleon transfer reactions, one can see Ref. [21].

Recently, experimental research on the transfer reaction in the $^{136}$Xe + $^{208}$Pb system at $E_{\mathrm{c.m.}} = 450$ MeV showed that the observed projectile-like fragments (PLFs) span the region from $Z = 48$ to $Z = 68$ while the observed target-like fragments (TLFs) range from $Z = 70$ to $Z = 88$ [14]. However, the nucleon transfer mechanism between projectile and target is still not clear. It requires theoretical models to understand some details in the nucleon transfer process. The neck dynamics plays a very important role in nucleon exchange and energy dissipation between the projectile and target at incident energy near the Coulomb barrier [22–24]. The nucleon exchange and the dissipation of the relative motion energy of the colliding nuclei occur in the neck region. Knowing how the excitation energy is divided between the two reaction partners is very important to understanding the energy dissipation mechanisms. Therefore, it is necessary to investigate the influence of the lifetime of the neck on the nucleon exchange and energy dissipation between the projectile and target.

*licheng@mail.bnu.edu.cn

†tianjunlong@gmail.com

‡wangning@gxnu.edu.cn

§Corresponding author: fszhang@bnu.edu.cn

 

To describe the multinucleon transfer process in low-energy heavy-ion collisions, some semiclassical and microscopic models are proposed. The semiclassical models such as the dinuclear system (DNS) [25–28], GRAZING [29–33], and complex WKB (CWKB) [34–37] have shown reasonable success in predicting the production cross sections of neutron-rich heavy nuclei in multinucleon transfer reactions. The GRAZING model, for example, incorporates the proper nuclear structure and dynamics information and describes the nucleon transfer processes via a multistep exchange of nucleons by stripping and pickup. It describes quite well a few nucleon transfer processes in $^{58}$Ni + $^{208}$Pb [38], $^{136}$Xe + $^{198}$Pt [39], and $^{136}$Xe + $^{238}$U [40] systems, and others.

To understand the dynamical mechanism in heavy-ion collisions, some microscopic dynamics models such as the time-dependent Hartree-Fock (TDHF) model [41–44] and the improved quantum molecular dynamics (ImQMD) model [45–47] have been developed. The ImQMD model is a semiclassical microscopic dynamics model which includes the mean-field and nucleon-nucleon collisions as well as the Pauli principle and is successfully applied to heavy-ion fusion reactions at energies near the Coulomb barrier [48] and intermediate-energy heavy-ion collisions [49,50]. To study the dynamic characters and energy dissipation of multinucleon transfer reactions, we apply the ImQMD model to simulate the multinucleon transfer process for the reaction of $^{136}$Xe + $^{208}$Pb at $E_{\rm c.m.} = 450$ MeV. The de-excitation process of primary fragments are treated with the GEMINI code.

The structure of this paper is as follows. In Sec. II, we briefly introduce the ImQMD model. In Sec. III, the dynamic characters and energy dissipation of the multinucleon transfer reaction for $^{136}$Xe + $^{208}$Pb at $E_{\rm c.m.} = 450$ MeV have been studied by using the ImQMD model. And then the mass distributions of the primary fragments and the isotope distributions of final fragments from Pt to At are calculated. The calculation results are compared with the experimental data as well as the calculations from the DNS and GRAZING models. Finally the conclusion is given in Sec. IV.

## II. MODEL

The ImQMD model is an improved version of the quantum molecular dynamics (QMD) model [51] which takes into account the effects of the surface term, the phase-space density constraint, and the surface-symmetry potential term. The nuclear interaction potential energy $U_{\rm loc}$ is obtained from the integration of the Skyrme energy density functional $U = \int V_{\rm loc}(\mathbf{r})d\mathbf{r}$ without the spin-orbit term, which reads

$$V_{\rm loc} = \frac{\alpha}{2}\frac{\rho^2}{\rho_0} + \frac{\beta}{\gamma+1}\frac{\rho^{\gamma+1}}{\rho_0^{\gamma}} + \frac{g_{\rm sur}}{2\rho_0}(\nabla\rho)^2 + \frac{C_s}{2\rho_0}[\rho^2 - \kappa_s(\nabla\rho)^2]\delta^2 + g_\tau\frac{\rho^{\eta+1}}{\rho_0^{\eta}}. \quad (1)$$

Here $\rho = \rho_n + \rho_p$ is the nucleon density. $\delta = (\rho_n - \rho_p)/(\rho_n + \rho_p)$ is the isospin asymmetry. The density distribution function $\rho$ of a system can be read as

$$\rho(r) = \sum_i \frac{1}{(2\pi\sigma_r)^{3/2}}\exp\left[-\frac{(\boldsymbol{r}-\boldsymbol{r}_i)^2}{2{\sigma_r}^2}\right]. \quad (2)$$

The $\sigma_r$ is the wave-packet width of nucleon. The parameters named IQ2 (see Table I) adopted in this work are the same as in Refs. [45,46] which have been tested for describing the heavy-ion collisions in fusion reactions, strongly damped reactions, and ternary breakup processes. To describe the fermionic nature of the $N$-body system and improve the stability of an individual nucleus, the Fermi constraint is adopted. The two-body collision correlations and the Pauli blocking checking at the next time step are also included.

TABLE I. Model parameters (IQ2) adopted in this work.

| $\alpha$ (MeV) | $\beta$ (MeV) | $\gamma$ | $g_{\rm sur}$ (MeV fm$^2$) | $g_\tau$ (MeV) | $\eta$ | $C_S$ (MeV) | $\kappa_s$ (fm$^2$) | $\rho_0$ (fm$^{-3}$) |
|---|---|---|---|---|---|---|---|---|
| −356 | 303 | 7/6 | 7.0 | 12.5 | 2/3 | 32.0 | 0.08 | 0.165 |

In this work, we set the $z$ axis as the beam direction and the $x$ axis as the impact parameter direction. The initial distance of the center of mass between the projectile and target is 30 fm. We use the parameter sets of IQ2 and set the wave-packet width $\sigma_r = 1.3$ fm to calculate the collision process of $^{136}$Xe + $^{208}$Pb at incident energy $E_{\rm c.m.} = 450$ MeV. The dynamic simulation is stopped at 2500 fm/$c$, then a statistical model (GEMINI code) is used to deal with the subsequent de-excitation process. The excitation energy of an excited fragment is obtained as the total energy of the fragment in the body frame with the corresponding ground-state binding energy subtracted. The GEMINI is a Monte Carlo code which follows the decay of a compound nuclei by a series of sequential binary decays until the resulting products are unable to undergo any further decay [52,53]. It allows not just light-particle emission and symmetric fission, but also the decaying nucleus to emit a fragment of any mass. The emission of light particles is described by the Hauser-Feshbach formalism, which explicitly treats and conserves angular momentum. The production of heavier fragment is described by Moretto binary decay formalism while the Bohr-Wheeler formalism is used for more symmetric fission of a heavy system. Nuclear level densities are taken as a Fermi-gas form with default parameters in this work.

## III. RESULTS AND DISCUSSION

### A. Dynamic characters and energy dissipation in transfer reactions

For this reaction, the incident energy in the center-of-mass frame is 450 MeV which is slightly higher than the Coulomb barrier (421.5 MeV), while the $Z_pZ_T$ value is 4428 which is much larger than the critical value (∼1600) of fusion reactions [54–57]. The projectile and target cannot form a compound nucleus due to strong Coulomb repulsion. The fusion-fission behavior cannot exist in the evolution process of systems. The formation of a neck between the projectile and target is the main character in the collision process. Figure 1

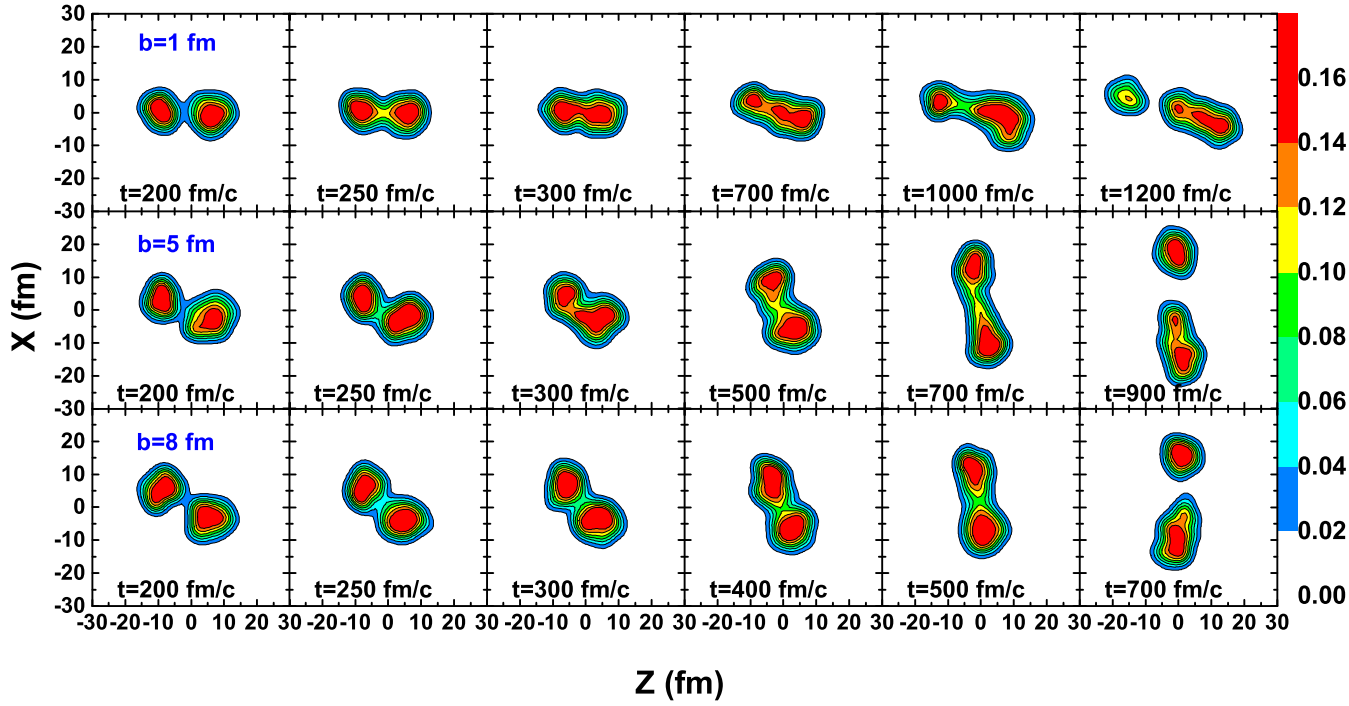


FIG. 1. Time evolution of density distribution for three typical events of the reaction $^{136}$Xe + $^{208}$Pb at $b = 1$ (top panels), 5 (middle panels), and 8 (bottom panels) fm.

shows the time evolution of density distribution for three typical events of the reaction $^{136}$Xe + $^{208}$Pb at $b = 1$,5, and 8 fm. We find a formation of a neck between the projectile and target during the collision. One can estimate the lifetime of the neck to be about 1000, 700, and 500 fm/$c$ for $b = 1$,5, and 8 fm, respectively. The lifetime of the neck decreases with increasing of impact parameters due to the contribution of the angular momentum of system. These are typical time scales for the transfer reactions, which are a $10^{-21}$ s order of magnitude. In addition, one can also find that there are two cores of density formed in the TLFs for $b = 1$ fm at $t = 1200$ fm/$c$ and for $b = 5$ fm at $t = 900$ fm/$c$. This is because a higher excited energy is obtained from the dissipation of the relative motion energy of the colliding nuclei in the central and semicentral collisions. It implies that the TLFs may be fission in the later evolution.

Figure 2(a) shows the lifetime of the neck calculated by the ImQMD model as a function of impact parameters. One can see that neck lifetime decreases with increasing impact parameters. Through a number of nucleon exchanges in the neck, the PLFs and TLFs are formed at the breakpoint. The nucleons in the PLFs (TLFs) consist of two parts: residual nucleons of the original projectile (target) and transferred nucleons from the target (projectile). Here we define a quantity $\eta = (\delta N_p - \delta N_t)/(\delta N_p + \delta N_t)$ to show the degree of nucleon exchange between two reaction partners, where $\delta N_p + \delta N_t$ is the total nucleon number of PLFs (or TLFs). $\delta N_p$ and $\delta N_t$ denote the nucleon numbers from the original projectile and target, respectively. In Fig. 2(b), we present $\eta$ as a function of impact parameters. One can see that the $\eta$ value increases for PLFs and decrease for TLFs with increasing of impact parameters. For the central collisions, a great many nucleons are exchanged between the projectile and target because the neck lifetime is very long. The $\eta$ value for both the PLFs and TLFs is close to $-0.21$ which is the value of the nucleon exchange equilibrium between the

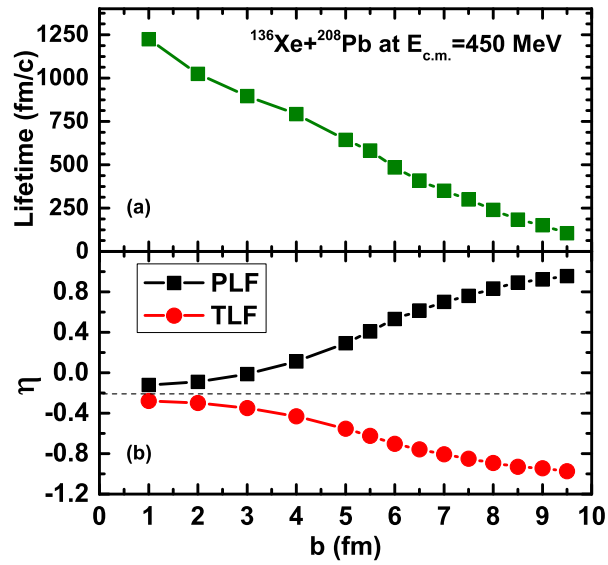


FIG. 2. (a) Lifetime of the neck calculated by the ImQMD model as a function of impact parameters. (b) Nucleon transfer ratio $\eta$ as a function of impact parameters. $\eta = (\delta N_p - \delta N_t)/(\delta N_p + \delta N_t)$, where $\delta N_p + \delta N_t$ is the total nucleon number of PLFs (or TLFs). $\delta N_p$ and $\delta N_t$ denote the number of nucleons that come from the original projectile and target, respectively. The dashed line denotes the value of the nucleon exchange equilibrium between the projectile and target which is $-0.21$.

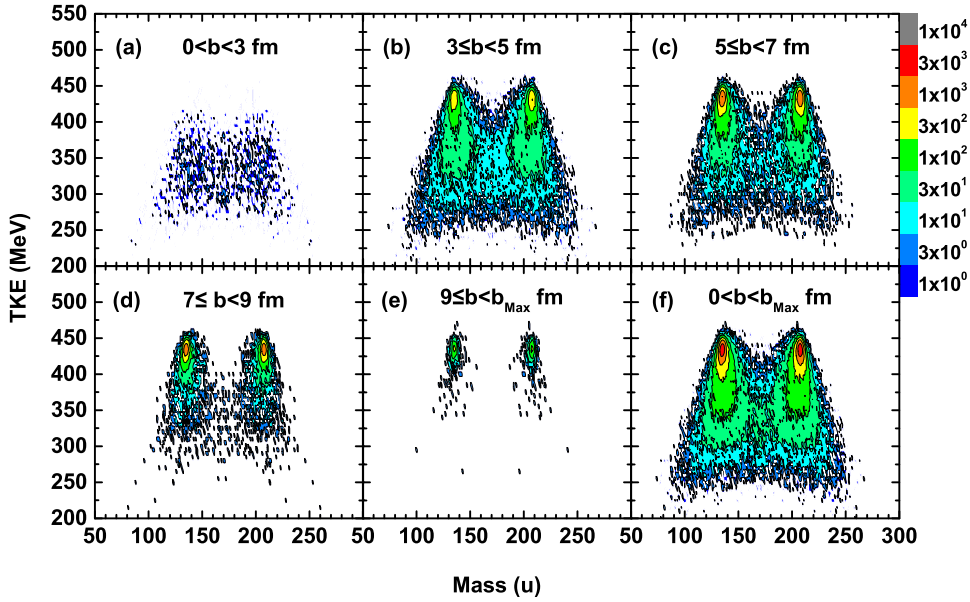


FIG. 3. TKE-mass distributions of primary binary fragments in different impact parameter regions.

projectile and target. The average length of time for reaching the nucleon exchange equilibrium is about 1200 fm/$c$. While for the peripheral collisions, the number of nucleon exchanges between the projectile and target decreases due to the short lifetime of the neck.

Figure 3 shows the total-kinetic-energy–mass distributions of primary binary fragments in different impact parameter regions. The total kinetic energy (TKE) is calculated in the center-of-mass system. From Fig. 3 one can see two behaviors: (1) The TKE has an increased trend with increasing impact parameters. For $0 < b < 3$ fm [Fig. 3(a)], the TKE is located in the region of $250 \sim 400$ MeV. The corresponding energy dissipation is about $200 \sim 50$ MeV, which indicates that central collisions are deep-inelastic reactions. For $3 \leqslant b < 5$ fm [Fig. 3(b)] and $5 \leqslant b < 7$ fm [Fig. 3(c)], the TKE is distributed over a wide range from 250 to 450 MeV. Both the deep-inelastic and quasielastic collision events appear in semicentral and semiperipheral collisions. This is because the dynamical fluctuation causes intense competition between the quasielastic and deep-inelastic reactions. For $7 \leqslant b$ fm [Figs. 3(d) and 3(e)], the TKE is gradually close to 450 MeV which indicates peripheral collisions correspond to quasielastic reactions. (2) The masses distribute in a rather broad range (80–250) in central to semiperipheral collisions [Figs. 3(a)–3(c)]. There are a large number of nucleon transfers between the projectile and target especially for deep-inelastic reaction events. While in peripheral collisions [Figs. 3(d) and 3(e)], there are only a few nucleon transfers between the projectile and target because the reaction mechanism is dominated by quasielastic collisions.

Figure 4 shows that the distribution of the total kinetic energy lost (TKEL, i.e., $E_{\text{c.m.}} - \text{TKE}$) for primary binary events. The solid circles denote all the binary events; the solid line denotes the Gaussian fitting for the quasielastic events. In Fig. 4 one can see that a Gaussian-type distribution appeared at TKEL values lower than 40 MeV, which correspond to quasielastic collision events. Most of the deep-inelastic events are located at TKEL values above 40 MeV. The TKEL distribution calculated by the ImQMD model is very similar to that measured by experiment [58] from reaction $^{88}\text{Sr} + ^{176}\text{Yb}$ at an incident energy slightly above the Bass barrier. It shows that the ImQMD model is also applicable for the study of energy dissipation in transfer reactions.

Now let us discuss the excitation energy division between the PLFs and TLFs in the multinucleon transfer reactions. In this work, we calculate the excitation energy as $E^* = E_f - E_b$. The $E_f$ and $E_b$ denote the total energy and ground-state energy for the PLFs or TLFs, respectively. In Fig. 5(a), we present the average excitation energy of the PLFs and TLFs as a function of neck lifetime by using the ImQMD model. One can see that the average excitation energy increases with increasing lifetime of the neck both for PLFs and TLFs. It also implies that the energy dissipation of the system is closely related to

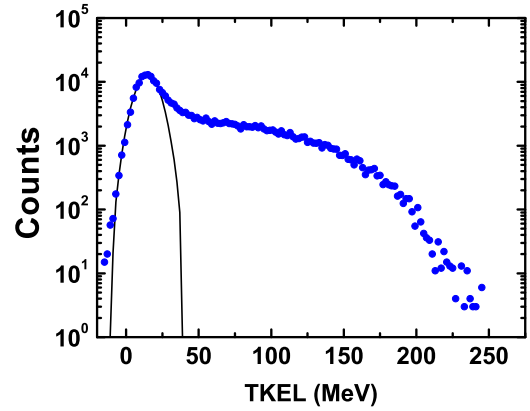


FIG. 4. TKEL distributions of primary binary fragments. The solid circles denote all the binary events; solid line denotes the Gaussian fitting for the quasielastic events.

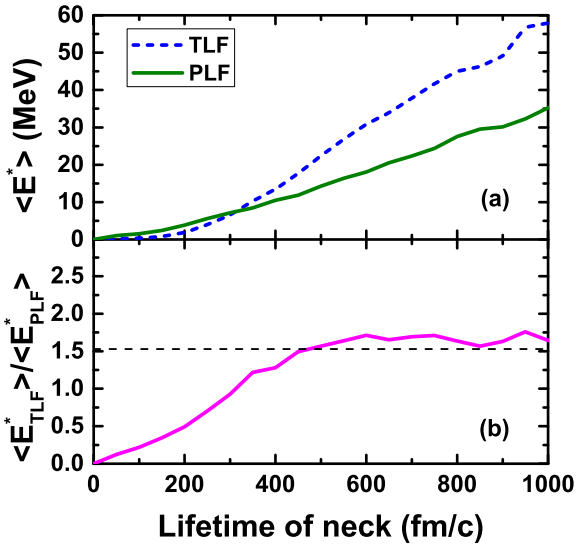


FIG. 5. (a) Average excitation energy of PLFs and TLFs as a function of neck lifetime. (b) $\langle E^*_{\rm TLF}\rangle/\langle E^*_{\rm TLF}\rangle$ as a function of neck lifetime. The dashed line denotes the value of thermal equilibrium between the TLFs and PLFs.

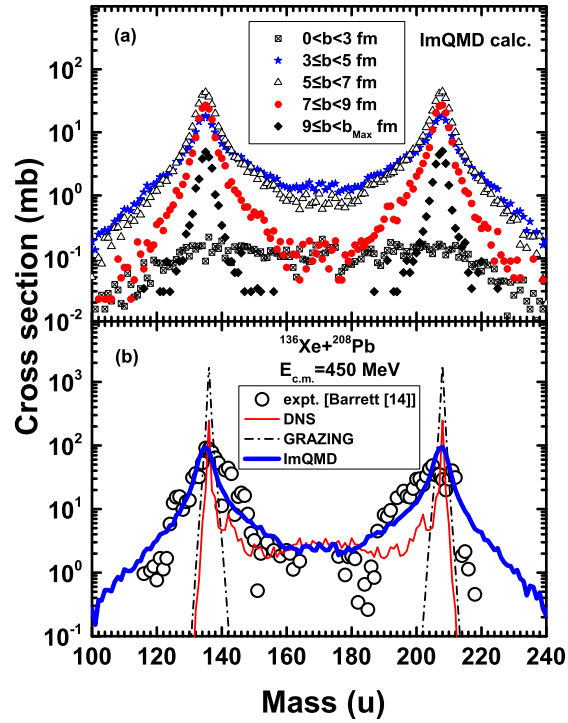


FIG. 6. (a) Mass distributions of primary binary fragments at different impact parameter regions from the ImQMD model. (b) Mass distributions of primary binary fragments calculated with the ImQMD (thick solid line), DNS (thin solid line), and GRAZING (dash-dot line) model. The experimental data (open circles) are from Ref. [14].

nucleon exchange between the projectile and target through the neck. In addition, one can also find that the excitation energy of the PLF is higher than the TLF in neck lifetimes less than 310 fm/$c$. This may be because lighter projectiles undergo larger Coulomb excitation in quasielastic collisions. With increasing neck lifetimes, the excitation energy of the TLF becomes higher than that of the PLF. The reason is that the relative motion energy of two colliding nuclei is dissipated by frequent nucleon exchanges. This will lead to PLFs that are less affected by the secondary process because the PLFs emit less neutrons than the TLFs in the deexcitation process. This phenomenon can be find in Ref. [38]. To better display the relationship of excitation energy between the TLFs and PLFs, we show the TLF to PLF excitation energy ratio as a function of neck lifetime in Fig. 5(b). The dashed line denotes the value of thermal equilibrium between the TLFs and PLFs which is approximately equal to the mass ratio of projectile to target. One can see that thermal equilibrium is reached at a neck lifetime above 480 fm/$c$, which is earlier than the nucleon exchange equilibrium (about 1200 fm/$c$).

### B. Mass distributions and isotopic distributions

The mass distributions of the primary fragments calculated with the ImQMD model in different impact parameter regions are shown in Fig. 6(a). One can see that for the regions of $3 \leqslant b < b_{\rm max}$ fm, the peak values are around the mass of the entrance channel, which also means that the quasielastic reaction makes an important contribution in semicentral to peripheral collisions. This is because the incident energy is slightly higher than the Coulomb barrier. The cross sections of $A < 128$, $144 < A < 200$, and $A > 216$ increase gradually with decreasing impact parameters. It is clear that the deep-inelastic collisions cause a large number of net nucleon transfers between the projectile and target. Due to the low-weight impact parameter and the sequential fission of excited fragments, the cross sections are very low in the whole mass region for $b < 3$ fm. The sum of cross sections with all impact parameters are shown in Fig. 6(b) and compared with the results of DNS and GRAZING [32,33] models. Here we use the GRAZING model with standard parameters. The experimental data (secondary fragments), which were derived from $\gamma$ intensities of a thick target experiment, from Ref. [14] are also shown in Fig. 6(b). One can see that the DNS and GRAZING models are only suitable to describe a few nucleon transfer processes between the projectile and target. For the ImQMD model, the experimental data can be reproduced very well in most of the mass regions.

The isotopic production cross sections with charge numbers from $Z = 78$ to 85 are shown in Fig. 7. The thick solid line, thin solid line, and dash-dot line denote the calculation results from the combinations of ImQMD + GEMINI and DNS + GEMINI, and from the GRAZING model with inclusion of evaporation for secondary fragments. The experiment data (secondary fragments) are taken from Ref. [14] which are denoted by solid circles. One can see that GRAZING is a suitable mode to estimate the production cross sections of the trans-target only for $\Delta Z = -1$ to $+2$. It grossly underestimates the production cross section by orders of magnitude in the case of more proton transfers. For example, for the Pt ($\Delta Z = -4$) isotopes, the estimated production cross sections are lower than $10^{-3}$ mb. Hence, it did not appear in the Fig. 7(a). For the combination of DNS + GEMINI, the height of peaks kept consistent with

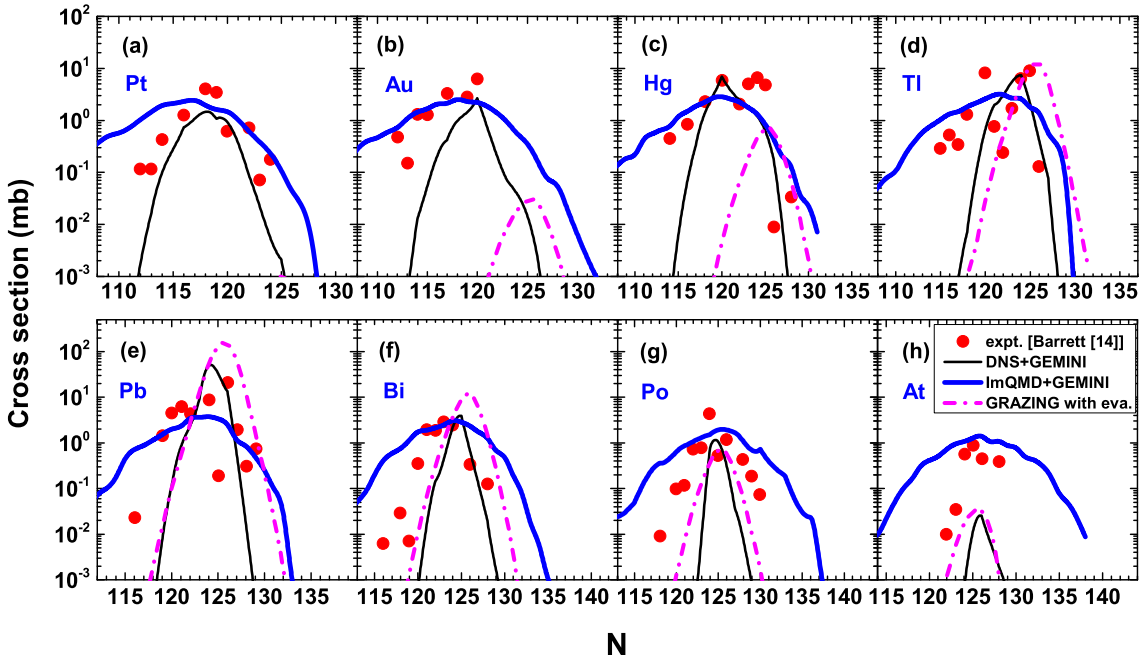


FIG. 7. Isotopic production cross sections from Pt to At. The thick solid line, thin solid line, and dash-dot line denote the calculation results from the combinations of ImQMD + GEMINI and DNS + GEMINI, and from the GRAZING model with inclusion of evaporation for secondary fragments. The experimental data (solid circles) are from Ref. [14].

experimental data at least on the orders of magnitude for $\Delta Z = -4$ to $+2$. However, it underestimates the cross section in the neutron-rich and neutron-deficient regions. In addition, the production cross sections decreases rapidly with increasing $\Delta Z$ in the region of charge numbers above 82 (Pb). For the combination of ImQMD + GEMINI, the height of peaks always kept consistent with experimental data for $\Delta Z = -4$ to $+3$, but the peak widths are usually greater than experimental data especially for $\Delta Z > 0$. There are flaws in describing larger neutron transfer. This may be because the neutrons are easier to transfer between the two reaction partners in the framework of ImQMD model. Even so, it is useful for estimating the production cross sections for $\Delta Z = -3$ to 0. In addition, note that the experimental data in Ref. [14] are derived from $\gamma$ intensities of a thick target experiment not from direct particle identification. There are probably some differences between the two measurement methods for isotope production cross sections.

## IV. CONCLUSIONS

The multinucleon transfer mechanisms for the reaction $^{136}$Xe + $^{208}$Pb at $E_{\mathrm{c.m.}} = 450$ MeV were studied by using the improved quantum molecular dynamics model. The lifetime of the neck plays an important role in the nucleon exchange and energy dissipation between the projectile and target during collisions. The degree of nucleon exchange between the projectile and target increases with increasing lifetime of the neck. The time of the nucleon exchange equilibrium is about 1200 fm/$c$. The total-kinetic-energy–mass distributions of primary binary fragments in different impact parameters regions are given. They show that the central collisions correspond to deep-inelastic collisions and the peripheral collisions correspond to quasielastic collisions. The excitation energy division between the PLFs and TLFs were also studied. We find that the lighter projectile is easier to excite in quasielastic collisions. The thermal equilibrium between two reaction partners is reached earlier than the nucleon exchange equilibrium. The primary fragment mass distributions are calculated by the ImQMD, DNS, and GRAZING models. To obtain the final isotope cross section distributions, GEMINI was employed to describe the de-excitation process of primary fragments. The result shows that GRAZING is a suitable mode to estimate the production cross sections of the trans-target for $\Delta Z = -1$ to $+2$, while the combination of DNS + GEMINI kept consistent with experimental data at least on the orders of magnitude for $\Delta Z = -4$ to $+2$. The combination of ImQMD + GEMINI is suitable to predict the isotopic production cross sections for $\Delta Z = -3$ to 0.

## ACKNOWLEDGMENTS

This work was supported by the National Natural Science Foundation of China under Grants No. 11025524, No. 11161130520, No. 11422548, No. 11275052, and No. 11475004; the National Basic Research Program of China under Grant No. 2010CB832903; and the European Commission's 7th Framework Programme (Fp7-PEOPLE-2010-IRSES) under Grant Agreement Project No. 269131.

[1] J. V. Kratz, A. E. Norris, and G. T. Seaborg, Phys. Rev. Lett. **33**, 502 (1974).

[2] K. D. Hildenbrand, H. Freiesleben, F. Pühlhofer, W. F. W. Schneider, R. Bock, D. V. Harrach, and H. J. Specht, Phys. Rev. Lett. **39**, 1065 (1977).

[3] M. Schädel, J. V. Kratz, H. Ahrens, W. Brüchle, G. Franz, H. Gäggeler, I. Warnecke, G. Wirth, G. Herrmann, N. Trautmann, and M. Weis, Phys. Rev. Lett. **41**, 469 (1978).

[4] M. Schädel, W. Brüchle, H. Gäggeler, J. V. Kratz, K. Sümmerer, G. Wirth, G. Herrmann, R. Stakemann, G. Tittel, N. Trautmann, J. M. Nitschke, E. K. Hulet, R. W. Lougheed, R. L. Hahn, and R. L. Ferguson, Phys. Rev. Lett. **48**, 852 (1982).

[5] R. B. Welch, K. J. Moody, K. E. Greorich, D. Lee, and G. T. Seaborg, Phys. Rev. C **35**, 204 (1987).

[6] K. J. Moody, D. Lee, R. B. Welch, K. E. Gregorich, G. T. Seaborg, R. W. Lougheed, and E. K. Hulet, Phys. Rev. C **33**, 1315 (1986).

[7] R. Künkel, W. V. Oertzen, B. Gebauer, H. G. Bohlen, H. A. Bösser, B. Kohlmeyer, F. Pühlhofer, and D. Schüll, Phys. Lett. B **208**, 355 (1988).

[8] Ch. Wennemann, W.-D. Schmidt-Ott, T. Hild, K. Krumbholz, V. Kunze, F. Meissner, H. Keller, R. Kirchner, and E. Roeckl, Z. Phys. A **347**, 185 (1994).

[9] K. Morita, K. Morimoto, D. Kaji, T. Akiyama, S. Goto, H. Haba, E. Ideguchi, R. Kanungo, K. Katori, H. Koura, H. Kudo, T. Ohnishi, A. Ozawa, T. Suda, K. Sueki, H. Xu, T. Yamaguchi, A. Yoneda, A. Yoshida, and Y. Zhao, J. Phys. Soc. Jpn. **73**, 2593 (2004).

[10] V. K. Utyonkov, N. T. Brewer, Yu. Ts. Oganessian, K. P. Rykaczewski, F. Sh. Abdullin, S. N. Dmitriev, R. K. Grzywacz, M. G. Itkis, K. Miernik, A. N. Polyakov, J. B. Roberto, R. N. Sagaidak, I. V. Shirokovsky, M. V. Shumeiko, Yu. S. Tsyganov, A. A. Voinov, V. G. Subbotin, A. M. Sukhov, A. V. Sabel'nikov, G. K. Vostokin, J. H. Hamilton, M. A. Stoyer, and S. Y. Strauss, Phys. Rev. C **92**, 034609 (2015).

[11] Y. T. Oganessian, V. K. Utyonkov, Y. V. Lobanov, F. S. Abdullin, A. N. Polyakov, I. V. Shirokovsky, Y. S. Tsyganov, G. G. Gulbekian, S. L. Bogomolov, B. N. Gikal, A. N. Mezentsev, S. Iliev, V. G. Subbotin, A. M. Sukhov, A. A. Voinov, G. V. Buklanov, K. Subotic, V. I. Zagrebaev, M. G. Itkis, J. B. Patin, K. J. Moody, J. F. Wild, M. A. Stoyer, N. J. Stoyer, D. A. Shaughnessy, J. M. Kenneally, and R. W. Lougheed, Nucl. Phys. A **734**, 109 (2004).

[12] S. J. Steer, Z. Podolyak, S. Pietri, M. Gorska, P. H. Regan, D. Rudolph, E. Werner-Malento, A. B. Garnsworthy, R. Hoischen, J. Gerl, H. J. Wollersheim, K. H. Maier, H. Grawe, F. Becker, P. Bednarczyk, L. Caceres, P. Doornenbal, H. Geissel, J. Grebosz, A. Kelic, I. Kojouharov, N. Kurz, F. Montes, W. Prokopowicz, T. Saito, H. Schaffner, S. Tashenov, A. Heinz, M. Pfützner, T. Kurtukian-Nieto, G. Benzoni, A. Jungclaus, D. L. Balabanski, C. Brandau, B. A. Brown, A. M. Bruce, W. N. Catford, I. J. Cullen, Z. Dombradi, M. E. Estevez, W. Gelletly, G. Ilie, J. Jolie, G. A. Jones, M. Kmiecik, F. G. Kondev, R. Krücken, S. Lalkovski, Z. Liu, A. Maj, S. Myalski, S. Schwertel, T. Shizuma, P. M. Walker, and O. Wieland, Phys. Rev. C **78**, 061302 (2008).

[13] M. H. Mun, G. G. Adamian, N. V. Antonenko, Y. Oh, and Y. Kim, Phys. Rev. C **91**, 054610 (2015).

[14] J. S. Barrett, W. Loveland, R. Yanez, S. Zhu, A. D. Ayangeakaa, M. P. Carpenter, J. P. Greene, R. V. F. Janssens, T. Lauritsen, E. A. McCutchan, A. A. Sonzogni, C. J. Chiara, J. L. Harker, and W. B. Walters, Phys. Rev. C **91**, 064615 (2015).

[15] H. M. Devaraja, S. Heinz, O. Beliuskina, V. Comas, S. Hofmann, C. Hornung, G. Münzenberg, K. Nishio, D. Ackermann, Y. K. Gambhir, M. Gupta, R. A. Henderson, F. P. Heßberger, J. Khuyagbaatar, B. Kindler, B. Lommel, K. J. Moody, J. Maurer, R. Mann, A. G. Popeko, D. A. Shaughnessy, M. A. Stoyer, and A. V. Yeremin, Phys. Lett. B **748**, 199 (2015).

[16] M. V. Pajtler, S. Szilner, L. Corradi, G. de Angelis, E. Fioretto, A. Gadea, F. Haas, S. Lunardi, D. J. Malenica, N. Mărginean, D. Mengoni, T. Mijatović, G. Montagnoli, D. Montanari, G. Pollarolo, F. Recchia, M. D. Salsac, F. Scarlassara, N. Soić, A. M. Stefanini, C. A. Ur, and J. J. Valiente-Dobón, Nucl. Phys. A **941**, 273 (2015).

[17] V. Zagrebaev and W. Greiner, Phys. Rev. Lett. **101**, 122701 (2008).

[18] W. Loveland, A. M. Vinodkumar, D. Peterson, and J. P. Greene, Phys. Rev. C **83**, 044610 (2011).

[19] V. I. Zagrebaev and W. Greiner, Phys. Rev. C **87**, 034608 (2013).

[20] V. I. Zagrebaev and W. Greiner, Phys. Rev. C **83**, 044618 (2011).

[21] L. Corradi, G. Pollarolo, and S. Szilner, J. Phys. G **36**, 113101 (2009).

[22] S. Ayik, O. Yilmaz, B. Yilmaz, A. S. Umar, A. Gokalp, G. Turan, and D. Lacroix, Phys. Rev. C **91**, 054601 (2015).

[23] S. Ayik, K. Washiyama, and D. Lacroix, Phys. Rev. C **79**, 054606 (2009).

[24] G. G. Adamian, N. V. Antonenko, and H. Lenske, Phys. Rev. C **91**, 054602 (2015).

[25] N. V. Antonenko, E. A. Cherepanov, A. K. Nasirov, V. P. Permjakov, and V. V. Volkov, Phys. Lett. B **319**, 425 (1993).

[26] G. G. Adamian, N. V. Antonenko, and W. Scheid, Nucl. Phys. A **618**, 176 (1997).

[27] L. Zhu, Z. Q. Feng, and F. S. Zhang, J. Phys. G **42**, 085102 (2015).

[28] G. G. Adamian, N. V. Antonenko, V. V. Sargsyan, and W. Scheid, Phys. Rev. C **81**, 057602 (2010).

[29] A. Winther, Nucl. Phys. A **572**, 191 (1994).

[30] A. Winther, Nucl. Phys. A **594**, 203 (1995).

[31] R. Yanez and W. Loveland, Phys. Rev. C **91**, 044608 (2015).

[32] http://nrv.jinr.ru/nrv/webnrv/grazing/.

[33] http://personalpages.to.infn.it/∼nanni/grazing/.

[34] E. Vigezzi and A. Winther, Ann. Phys. (NY) **192**, 432 (1989).

[35] L. Corradi, J. H. He, D. Ackermann, A. M. Stefanini, A. Pisent, S. Beghini, G. Montagnoli, F. Scarlassara, G. F. Segato, G. Pollarolo, C. H. Dasso, and A. Winther, Phys. Rev. C **54**, 201 (1996).

[36] L. Corradi, A. M. Stefanini, D. Ackermann, S. Beghini, G. Montagnoli, C. Petrache, F. Scarlassara, C. H. Dasso, G. Pollarolo, and A. Winther, Phys. Rev. C **49**, R2875(R) (1994).

[37] S. Szilner, L. Corradi, G. Pollarolo, S. Beghini, R. B. Behera, E. Fioretto, A. Gadea, F. Haas, A. Latina, G. Montagnoli, F. Scarlassara, A. M. Stefanini, M. Trotta, A. M. Vinodkumar, and Y. Wu, Phys. Rev. C **71**, 044610 (2005).

[38] L. Corradi, A. M. Vinodkumar, A. M. Stefanini, E. Fioretto, G. Prete, S. Beghini, G. Montagnoli, F. Scarlassara, G. Pollarolo, F. Cerutti, and A. Winther, Phys. Rev. C **66**, 024606 (2002).

[39] Y. X. Watanabe, Y. H. Kim, S. C. Jeong, Y. Hirayama, N. Imai, H. Ishiyama, H. S. Jung, H. Miyatake, S. Choi, J. S. Song, E. Clement, G. de France, A. Navin, M. Rejmund, C. Schmitt, G. Pollarolo, L. Corradi, E. Fioretto, D. Montanari, M. Niikura, D. Suzuki, H. Nishibata, and J. Takatsu, Phys. Rev. Lett. **115**, 172503 (2015).

[40] A. Vogt, B. Birkenbach, P. Reiter, L. Corradi, T. Mijatović, D. Montanari, S. Szilner, D. Bazzacco, M. Bowry, A. Bracco, B. Bruyneel, F. C. L. Crespi, G. de Angelis, P. Désesquelles, J. Eberth, E. Farnea, E. Fioretto, A. Gadea, K. Geibel, A. Gengelbach, A. Giaz, A. Görgen, A. Gottardo, J. Grebosz, H. Hess, P. R. John, J. Jolie, D. S. Judson, A. Jungclaus, W. Korten, S. Leoni, S. Lunardi, R. Menegazzo, D. Mengoni, C. Michelagnoli, G. Montagnoli, D. Napoli, L. Pellegri, G. Pollarolo, A. Pullia, B. Quintana, F. Radeck, F. Recchia, D. Rosso, E. Şahin, M. D. Salsac, F. Scarlassara, P.-A. Söderström, A. M. Stefanini, T. Steinbach, O. Stezowski, B. Szpak, Ch. Theisen, C. Ur, J. J. Valiente-Dobón, V. Vandone, and A. Wiens, Phys. Rev. C **92**, 024619 (2015).
[41] P. Bonche, S. Koonin, and J. W. Negele, Phys. Rev. C **13**, 1226 (1976).
[42] K. T. R. Davies, K. R. Sandhya Devi, and M. R. Strayer, Phys. Rev. C **20**, 1372 (1979).
[43] K. Sekizawa and K. Yabana, Phys. Rev. C **88**, 014614 (2013).
[44] K. Sekizawa and K. Yabana, Phys. Rev. C **90**, 064614 (2014).
[45] J. L. Tian, X. Z. Wu, K. Zhao, Y. X. Zhang, and Z. X. Li, Phys. Rev. C **77**, 064603 (2008).
[46] K. Zhao, Z. X. Li, N. Wang, Y. X. Zhang, Q. F. Li, Y. J. Wang, and X. Z. Wu, Phys. Rev. C **92**, 024613 (2015).
[47] N. Wang, K. Zhao, and Z. X. Li, Phys. Rev. C **90**, 054610 (2014).
[48] N. Wang, L. Ou, Y. X. Zhang, and Z. X. Li, Phys. Rev. C **89**, 064601 (2014).
[49] C. Li, J. L. Tian, L. Ou, and N. Wang, Phys. Rev. C **87**, 064615 (2013).
[50] L. H. Mao, N. Wang, and L. Ou, Phys. Rev. C **91**, 044604 (2015).
[51] J. Aichelin, Phys. Rep. **202**, 233 (1991).
[52] R. J. Charity, M. A. McMahan, G. J. Wozniak, R. J. McDonald, L. G. Moretto, D. G. Sarantites, L. G. Sobotka, G. Guarino, A. Pantaleo, L. Fiore, A. Gobbi, and K. D. Hildenbrand, Nucl. Phys. A **483**, 371 (1988).
[53] R. J. Charity, Phys. Rev. C **82**, 014610 (2010).
[54] K.-H. Schmidtt and W. Morawek, Rep. Prog. Phys. **54**, 949 (1991).
[55] C. Y. Wong, Phys. Rev. Lett. **31**, 766 (1973).
[56] C. W. Shen, D. Boilley, Q. F. Li, J. J. Shen, and Y. Abe, Phys. Rev. C **83**, 054620 (2011).
[57] D. Boilley, H. L. Lü, C. W. Shen, Y. Abe, and B. G. Giraud, Phys. Rev. C **84**, 054608 (2011).
[58] E. M. Kozulin, G. N. Knyazheva, S. N. Dmitriev, I. M. Itkis, M. G. Itkis, T. A. Loktev, K. V. Novikov, A. N. Baranov, W. H. Trzaska, E. Vardaci, S. Heinz, O. Beliuskina, and S. V. Khlebnikov, Phys. Rev. C **89**, 014614 (2014).